Self-consistent random phase approximation and optimized hybrid functionals for solids

Thomas Pitts, Damian Contant, and Maria Hellgren Sorbonne Université, MNHN, UMR CNRS 7590, IMPMC, 4 place Jussieu, 75005 Paris, France (Dated: April 18, 2025)

The random phase approximation (RPA) and the GW approximation share the same total energy functional but RPA is defined on a restricted domain of Green's functions determined by a local Kohn-Sham (KS) potential. In this work, we perform self-consistent RPA calculations by optimizing the local KS potential through the optimized effective potential equation. We study a number of solids (C, Si, BN, LiF, MgO, TiO₂), and find in all cases a lowering of the total energy with respect to non-self-consistent RPA. We then propose a variational approach to optimize PBE0-type hybrid functionals based on the minimization of the RPA total energy with respect to the fraction of exact exchange used to generate the input KS orbitals. We show that this scheme leads to hybrid functionals with a KS band structure in close agreement with RPA, and with lattice constants of similar accuracy as within RPA. Finally, we evaluate G_0W_0 gaps using RPA and hybrid KS potentials as starting points. Special attention is given to TiO₂, which exhibits a strong starting-point dependence.

I. INTRODUCTION

The random phase approximation (RPA) within Kohn-Sham (KS) density functional theory (DFT) has become an important approach in chemistry and materials science, owing to its ability to accurately handle complex systems with mixed van der Waals/covalent bonds [1–16]. Studies have also shown that the RPA captures certain effects of strong electronic correlation [17–20]. Although most calculations are successfully employed nonself-consistently, i.e., the RPA energy is evaluated on top of the ground state of a simpler functional, reaching self-consistency is desirable as it provides an unbiased solution and gives access to interaction-induced changes in the ground-state density. Being diagrammatically equivalent to the GW approximation, the RPA density is expected to be similar to the GW density [21, 22].

Self-consistent calculations through the RPA KS potential have so far been performed on atoms [23] and small molecules [24–26]. These calculations have demonstrated that the RPA correlation potential exhibits several important features of the exact correlation potential. These include the atomic shell oscillations [23, 27, 28], the $\alpha/2r^4$ asymptotic tail [29], and the correlation peak that appears when dissociating a covalent bond [20, 25, 30]. These features, completely absent in local and semi-local approximations, can be attributed to the dependency of the RPA functional on both the occupied and unoccupied KS orbitals [31]. In addition, inter-shell-peaks due to exchange interactions are well described since the exchange term is treated exactly within RPA. The same property is also approximately captured by nonlocal functionals with a dependency on the occupied KS orbitals such as hybrid and meta-GGA (generalized gradient approximation) functionals [32, 33].

Early calculations on semiconductors were only partially self-consistent [34, 35], or employed the quasiparticle approximation [36]. Only recently was it shown that these approximations may strongly influence the results,

particularly the quasiparticle approximation [37]. Nevertheless, these works confirm that the RPA KS potential underestimates the band gap in solids, and that the derivative discontinuity of the exchange-correlation energy is large, corresponding to around 30%-50% of the gap [35, 38, 39]. This is not surprising given that the KS potential is designed to reproduce the density of the interacting system [40]. As such, the KS orbitals and eigenvalues (except for the highest occupied [41]) do not have a rigorous physical meaning and should, therefore, not be interpreted as excited states of the interacting system.

On the other hand, the KS system often represents a good starting point for calculating absorption spectra within time-dependent DFT [42, 43] and quasi-particle spectra within many-body perturbation theory [44–46]. Since RPA and GW share the same total energy functional, it is possible to show that the RPA KS band structure provides an optimal starting point for perturbative G_0W_0 band structure calculations [47]. At the same time, the G_0W_0 gap becomes equal to the RPA gap, calculated from the derivative of the RPA total energy with respect to the number of particles. The RPA potential is thus an interesting alternative to fully self-consistent GW, which is technically difficult to achieve due to the non-Hermitian and frequency-dependent GW selfenergy. Indeed, various quasi-self-consistent approaches have been proposed over the years to overcome this problem; self-consistency through the Green's function only, keeping the screened interaction fixed [48], quasiparticle self-consistency via a static approximation to the GW self-energy [49], and quasi-self-consistent approaches based on the simultaneous optimization of a parameterdependent Hubbard [50] or hybrid functional [51–53]. In this context, the RPA starting point stands out as it requires no approximation from a DFT perspective, at least for the evaluation of the band gap.

The RPA, just like hybrid and meta-GGA functionals, is an implicit functional of the density. There is thus not

an analytical expression for the exchange-correlation potential, which complicates its numerical evaluation. Instead, in each iteration towards self-consistency, one has to solve an integral equation known as the optimized effective potential (OEP) equation [54, 55]. Although numerically challenging, there exists a number of stable implementations both with plane-waves [24, 56, 57] and localized basis sets [23, 28, 58–60].

In this work, we evaluate the RPA KS potential for a set of solids (C, Si, BN, LiF, MgO, TiO_2) by generalizing a plane-wave implementation previously applied to molecules [24]. The RPA KS potential is then used to study starting-point dependencies within RPA and G_0W_0 . In all cases considered, we find that the RPA total energy has a well-defined minimum, and propose a variational approach for optimizing parameter-dependent hybrid functionals. This approach is compared to our previously proposed method based on quasi-self-consistency for the G_0W_0 band gap [53]. Focusing then on the PBE0 hybrid functional, we show that, for these weakly correlated solids, the resulting hybrid KS potentials accurately mimic the RPA KS potentials, yielding similar band structures, lattice constants and RPA band gaps.

The paper is organized as follows. In Sec. II, we review the basic equations of self-consistent RPA and derive two different RPA-based approaches for optimizing the exact-exchange fraction in hybrid functionals. In Sec. III, we present the computational setup and discuss results for KS potentials, lattice constants and RPA/G_0W_0 gaps. Finally, in Sec. IV, we give our conclusions.

II. THEORY AND IMPLEMENTATION

In this section, we review the equations for self-consistent RPA and their implementation based on an eigendecomposition of the KS linear density response function [24, 61]. We also discuss ways to achieve quasi-self-consistency within RPA while simultaneously optimizing parameter-dependent hybrid functionals.

A. Self-consistent RPA

The RPA correlation energy functional can be derived within many-body perturbation theory as a partial resummation of ring diagrams equivalent to those of the GW approximation [21, 22, 62, 63]. However, while the diagrams in GW are evaluated with a dressed Green's function, in RPA they are evaluated with an independent-particle Green's function, G_s . The final expression can either be written in terms of G_s or in terms of the independent-particle linear density response function, $\chi_s = -iG_sG_s$. In the latter case, we can write

$$E_{\rm c}^{\rm RPA} = \int_0^\infty \frac{d\omega}{2\pi} \text{Tr}\{\ln[1 - v\chi_s(i\omega)] + v\chi_s(i\omega)\}, \quad (1)$$

where v is the Coulomb interaction, and $Tr\{AB\} =$ $\int d\mathbf{r}d\mathbf{r}' A(\mathbf{r},\mathbf{r}') B(\mathbf{r}',\mathbf{r}).$ Combined with the exactexchange (EXX) energy functional, it provides a well-defined orbital-dependent exchange-correlation (xc) functional within the KS DFT framework. Although most calculations are done on top of the ground state of another functional, i.e., χ_s is constructed from the eigenvalue spectrum of, e.g., PBE (Perdew-Burke-Ernzerhof) [64, 65] or LDA (local density approximation), full selfconsistency, via a local xc potential, $v_{xc} = \delta E_{xc}/\delta n$, can also be achieved. However, since the dependence on the density is only implicit, the functional derivative of the xc energy with respect to the density must be evaluated using the chain rule through the total KS potential, $V_s = v_{\rm ext} + v_{\rm H} + v_{\rm xc}$, where 'ext' and 'H' stand for external and Hartree, respectively. This implies solving the OEP equation [54, 55]

$$\int d\mathbf{r}' \chi_s(\mathbf{r}, \mathbf{r}', \omega = 0) v_{\rm xc}(\mathbf{r}') = \frac{\delta E_{\rm xc}}{\delta V_s(\mathbf{r})}.$$
 (2)

The OEP equation is well-known from EXX theory, where expressions for the right hand side can be found in many works (see for example Refs. [66, 67]). The RPA correlation contribution can be evaluated as $\delta E_{\rm c}^{\rm RPA}/\delta \chi_s \times \delta \chi_s/\delta V_s$ [29], giving

$$\frac{\delta E_{\rm c}}{\delta V_s(\mathbf{r})} = -\int_0^\infty \frac{d\omega}{2\pi} \text{Tr} \left\{ \frac{vD(\mathbf{r}, i\omega)v\chi_s(i\omega)}{1 - v\chi_s(i\omega)} \right\}, \quad (3)$$

where

$$D(\mathbf{r}, i\omega) = \frac{\delta \chi_s(i\omega)}{\delta V_s(\mathbf{r})}.$$
 (4)

An expression for D in terms of KS orbitals and eigenvalues is given in the Appendix.

Implementations of the OEP equation for RPA exist for atoms in a spline basis set [23, 68], for molecules within Gaussian basis sets [26], and for solids within the PAW (projected augmented wave) framework [37]. In this work, we start from an existing plane-wave implementation within the ACFDT (adiabatic connection fluctuation dissipation theory) package of the Quantum ESPRESSO (QE) distribution [24, 61, 69]. In this implementation, $v\chi_s$, or more precisely $v^{1/2}\chi_s v^{1/2}$, is decomposed in terms of its eigenvalues v_β and eigenvectors V^β . The lowest eigenvalues, at every momentum ${\bf q}$ and imaginary frequency $i\omega$, are obtained by iterative diagonalization of the generalized eigenvalue problem

$$\chi_s(\mathbf{q}, i\omega)|V_{\mathbf{q}}^{\beta}\rangle = \nu_{\beta}(\mathbf{q}, i\omega)v_{\mathbf{q}}^{-1}|V_{\mathbf{q}}^{\beta}\rangle.$$
 (5)

The action of χ_s on a trial eigenvector (or "eigenpotential") is nothing but a density response, which can conveniently be determined within density functional perturbation theory (DFPT) [70, 71].

With the eigendecomposition of χ_s , the correlation en-

ergy in Eq. (1) reduces to a simpler expression

$$E_c = \frac{1}{N_{\mathbf{q}}} \sum_{\mathbf{q}} \int_0^\infty \frac{d\omega}{2\pi} \sum_{\beta}^{N_{\nu}} \ln[1 - \nu_{\beta}(\mathbf{q}, i\omega)] + \nu_{\beta}(\mathbf{q}, i\omega).$$

Similarly, the derivative (see (Eq. (3)) is given by

$$\frac{\delta E_c}{\delta V_s(\mathbf{r})} = -\frac{1}{N_{\mathbf{q}}} \sum_{\mathbf{q}} \int_0^\infty \frac{d\omega}{2\pi} \sum_{\beta}^{N_{\nu}} \frac{D_{\mathbf{q}}^{\beta}(\mathbf{r}, i\omega)\nu_{\beta}(\mathbf{q}, i\omega)}{1 - \nu_{\beta}(\mathbf{q}, i\omega)}, (7)$$

where

$$D_{\mathbf{q}}^{\alpha}(\mathbf{r}, i\omega) = 2 \sum_{\mathbf{k}n}^{\text{occ}} \varphi_{n\mathbf{k}}^{*}(\mathbf{r}) \delta \varphi_{n\mathbf{k}}^{1}(\mathbf{r}) + c.c.$$

$$-2 \sum_{\mathbf{k}n}^{\text{occ}} \varphi_{n\mathbf{k}+\mathbf{q}}^{*}(\mathbf{r}) \delta \varphi_{n\mathbf{k}+\mathbf{q}}^{2}(\mathbf{r}) + c.c.$$

$$-2 \sum_{\mathbf{k}nn'\sigma}^{\text{occ}} \langle \Delta^{\alpha} \varphi_{n\mathbf{k}+\mathbf{q}}^{-\sigma} | \Delta^{\alpha} \varphi_{n'\mathbf{k}+\mathbf{q}}^{\sigma} \rangle$$

$$\times \varphi_{n\mathbf{k}}(\mathbf{r}) \varphi_{n'\mathbf{k}}^{*}(\mathbf{r})$$

$$+2 \sum_{\mathbf{k}n\sigma}^{\text{occ}} \Delta^{\alpha} \varphi_{n\mathbf{k}+\mathbf{q}}^{\sigma}(\mathbf{r}) [\Delta^{\alpha} \varphi_{n\mathbf{k}+\mathbf{q}}^{-\sigma}(\mathbf{r})]^{*} (8)$$

and

$$|\Delta^{\alpha} \varphi_{n\mathbf{k}+\mathbf{q}}^{\sigma}\rangle = \sum_{m}^{\text{unocc}} |\varphi_{m\mathbf{k}+\mathbf{q}}\rangle \frac{\langle \varphi_{m\mathbf{k}+\mathbf{q}} | V_{\mathbf{q}}^{\alpha} | \varphi_{n\mathbf{k}}\rangle}{\sigma\omega + \varepsilon_{n\mathbf{k}} - \varepsilon_{m\mathbf{k}+\mathbf{q}}}$$
(9)

$$|\delta \varphi_{n\mathbf{k}}^{1}\rangle = \sum_{m}^{\text{unocc}} |\varphi_{m\mathbf{k}}\rangle \frac{\langle \varphi_{m\mathbf{k}}|V_{-\mathbf{q}}^{\alpha}|\Delta^{\alpha}\varphi_{n\mathbf{k}+\mathbf{q}}\rangle}{\varepsilon_{n\mathbf{k}} - \varepsilon_{m\mathbf{k}}}$$
(10)

$$|\delta\varphi_{n\mathbf{k}+\mathbf{q}}^{2}\rangle = \sum_{m}^{\text{unocc}} \sum_{m'\sigma}^{\text{occ}} |\varphi_{m\mathbf{k}+\mathbf{q}}\rangle \frac{\langle \varphi_{m\mathbf{k}+\mathbf{q}} | \Delta^{\alpha} \varphi_{m'\mathbf{k}+\mathbf{q}}^{\sigma} \rangle}{\varepsilon_{n\mathbf{k}+\mathbf{q}} - \varepsilon_{m\mathbf{k}+\mathbf{q}}} \times \langle \varphi_{m'\mathbf{k}} | V_{-\mathbf{q}}^{\alpha} | \varphi_{n\mathbf{k}+\mathbf{q}} \rangle. \tag{11}$$

The quantities in Eqs. (9-11) can be determined using DFPT. Furthermore, since $\delta E_{\rm x}/\delta V_s$ is equal to the density response of the Fock exchange potential and the left-hand side of Eq. (2) is equal to the density response of $v_{\rm xc}$, DFPT can also be used to evaluate the terms in Eq. (2). Using this computational scheme, combined with an iterative approach for solving the OEP equation [24, 72], accurate RPA xc potentials have been generated for molecules [24]. The same approach was also successfully employed to generate EXX potentials for solids [53]. In this work, we use a modified version of the ACFDT package of QE and generalize the implementation of the RPA potentials to solids.

The RPA total energy functional has a minimum at the OEP stationary point, provided the static density response function within self-consistent RPA has negative eigenvalues [73]. This cannot be proven in general but no

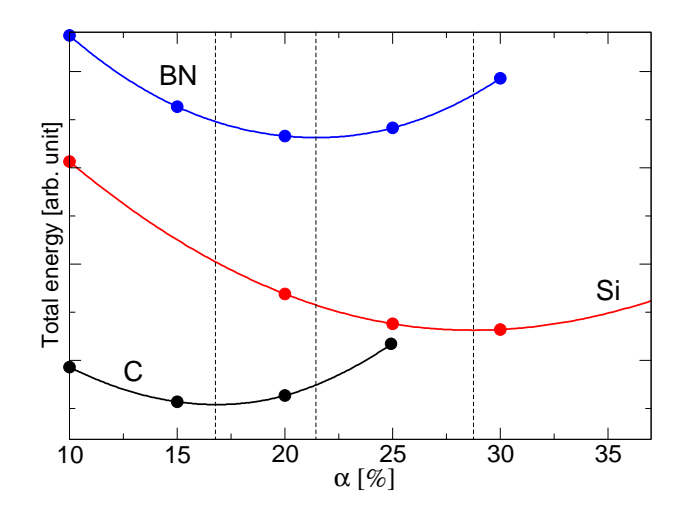


Figure 1. RPA total energy of C, BN, and Si, evaluated on top of an OEP α hybrid functional density, plotted as a function of α . The minima are marked with dashed vertical lines. The curves have been vertically shifted to fit on the same plot.

counter example has so far been found. The variational property of RPA can then be used to optimize computationally cheaper parameter-dependent approximations such as hybrid functionals, through a constrained minimization. For example, in the PBE0 α functional, the fraction (%) of exact exchange, α , included within PBE0 [74], is allowed to vary. By evaluating the RPA total energy on top of OEP-PBE0 α KS orbitals (an approximation from now on denoted OEP α to distinguish it from the more "standard" PBE0 α functional that uses a non-local exchange potential), we can locate the optimal α value by setting

$$\frac{dE[V_s^{\text{OEP}\alpha}]}{d\alpha} = 0. \tag{12}$$

The RPA-optimized hybrid KS potential, $V_s^{\text{OEP}\alpha_{\text{RPA}}}$, is expected to yield KS orbitals and eigenvalues similar to the self-consistent RPA potential, V_s^{RPA} . This approach was tested on molecules in Refs. [57, 75, 76] and shown to give reasonable values for α .

B. RPA band gap

The RPA is an approximation to the ground-state energy. The RPA band gap, defined as the difference between the ionization energy and the affinity, $E_g = I - A$, can be obtained from the derivative of the RPA ensemble energy with respect to the number of particles [47, 77]. This derivative is discontinuous at integer particle numbers; the derivative on the left-side equals the negative of the ionization energy

$$-I = \varepsilon_v + \langle v | \Sigma_s^{GW}(\varepsilon_v) - v_{\rm xc}^{\rm RPA} | v \rangle$$
 (13)

and the derivative on the right hand side equals the negative of the affinity

$$-A = \varepsilon_c + \langle c | \Sigma_s^{GW}(\varepsilon_c) - v_{xc}^{\text{RPA}} | c \rangle. \tag{14}$$

The GW self-energy appears here, confirming the close connection between RPA and GW. The labels v and c denote the RPA KS valence and conduction band states, respectively, and $v_{\rm xc}^{\rm RPA}$ is the xc part of the RPA KS potential. Equations (13) and (14) are valid only when the OEP equation (Eq. (2)) is fulfilled. These equations are identical to the expressions used in G_0W_0 calculations based on a KS reference system [36, 47, 53], except for the renormalization factor that is usually multiplied to the matrix element.

Analogous formulas can be derived for PBE0 α evaluated with an OEP α ground state. The GW self-energy is replaced by the nonlocal hybrid potential, which we here denote $\Sigma_s^{\mathrm{PBE0}\alpha}$, and the RPA potential is replaced by the local hybrid xc potential $v_{\mathrm{xc}}^{\mathrm{OEP}\alpha}$, obtained as the solution to the corresponding hybrid OEP equation. In Ref. [53], this similarity was used to evaluate Eqs. (13) and (14) approximately by replacing $v_{\mathrm{xc}}^{\mathrm{RPA}}$ with $v_{\mathrm{xc}}^{\mathrm{OEP}\alpha}$. Enforcing the RPA gap to equal the gap of the OEP α hybrid functional yields

$$\langle c|\Sigma_s^{GW}(\varepsilon_c) - \Sigma_s^{\text{PBE}0\alpha}|c\rangle - \langle v|\Sigma_s^{GW}(\varepsilon_v) - \Sigma_s^{\text{PBE}0\alpha}|v\rangle = 0, \qquad (15)$$

where the valence and conduction states are now given by $OEP\alpha$. In addition to generating an approximate starting point for G_0W_0 calculations, this scheme provides an alternative approach for optimizing the α -parameter. The optimal fraction of exact exchange fulfilling Eq. (15) will from now on be denoted $\alpha_{\rm opt}$ to distinguish it from the value $\alpha_{\rm RPA}$ obtained by fulfilling Eq. (12). Having access to the RPA potential, we will, in the next section, compare the results obtained from these two different approaches to the results obtained using the true RPA potential.

III. APPLICATIONS

In this section, we present the computational setup and show results obtained on a set of solids (C, Si, BN, LiF, MgO, rutile-TiO₂). We determine the self-consistent RPA potential and the optimal RPA fraction of exchange within the PBE0 α hybrid functional, using the two approaches described in Sec. II. The performance of the RPA and the optimized hybrid functionals is evaluated by looking at densities, KS band structures, lattice constants, and RPA/ G_0W_0 gaps.

A. Computational details

Most calculations were performed within the QE software. We used PBE optimized norm-conserving Vanderbilt (ONCV) pseudo potentials throughout this work

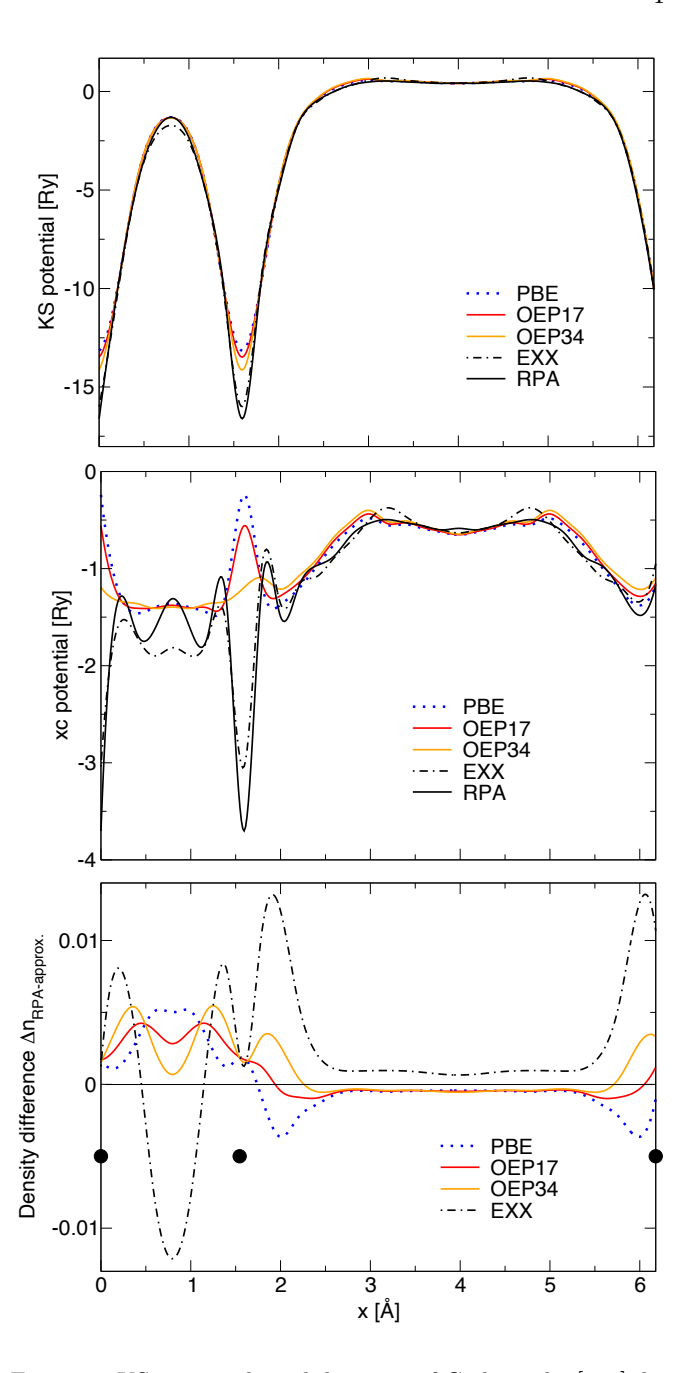


Figure 2. KS potentials and densities of C along the [111] direction. Top panel: total KS potential calculated using PBE, EXX, RPA, optimized OEP17, and OEP34. Middle panel: the xc part of the KS potentials. Bottom panel: density difference $\Delta n_{\rm RPA-approx.}$, where "approx." corresponds to PBE, EXX, OEP17, and OEP34. The positions of the carbon atoms are marked with black dots.

[78]. Lattice constants were determined with a plane-wave cutoff of 110 Ry and a $8\times8\times8/5\times5\times5$ (shifted) k-point grid for PBE0/RPA, respectively. KS band gaps were converged within 0.02 eV with a plane-wave cut-off of 80 Ry and a $6\times6\times6$ k-point grid. The RPA KS gaps converged quickly with the number of eigenvalues in the response function, approximately 5 times the number of

Table I. KS band gaps (eV) of C, Si, BN, LiF, MgO, and rutile TiO_2 , between Γ and different k-points. Results for EXX and RPA are compared to previous calculations reported in the literature. The approximation $OEP\alpha_{RPA}$ corresponds to the RPA optimized hybrid functional, with the optimal value for α (%) given in the preceding column. The MAE/MARE are determined with respect to the RPA result obtained in this work. Results marked with (*) or (†) are the approximate RPA calculations from Ref. [35] and Ref. [36], respectively.

Solid	k	PBE	EXX	EXX lit. ^a	RPA	RPA lit. ^b	$\alpha^{ ext{RPA}}$	$OEP\alpha_{RPA}$
С								
	Γ	5.60	6.20	6.20	5.76	5.75	17	5.67
	\mathbf{L}	8.47	9.07	9.07	8.63	8.62		8.54
	X	4.81	5.36	5.36	4.89	4.89		4.84
Si								
	Γ	2.56	3.18	3.15	2.71	2.68	29	2.68
	$_{ m L}$	1.52	2.21	2.29	1.62	1.64		1.66
	X	0.69	1.37	1.35	0.80	0.74		0.78
BN								
	Γ	8.80	9.72	9.80	9.01	9.12	22	8.96
	\mathbf{L}	10.19	11.07	11.19	10.32	10.37		10.34
	X	4.54	5.57	5.57	4.73	4.70		4.67
LiF								
	Γ	9.25	11.28	11.33	9.81	$9.5*/10.21^{\dagger}$	26	9.75
	\mathbf{L}	10.92	13.08	13.11	11.58	$11.3*/11.86^{\dagger}$		11.47
	X	14.95	16.97	17.02	15.65	$15.6*/15.88^{\dagger}$		15.46
$_{ m MgO}$								
	Γ	4.77	6.60	6.55	5.21	5.23	24	5.15
	\mathbf{L}	7.93	9.64	9.71	8.30	8.36		8.28
	X	9.19	10.88	10.88	9.55	9.50		9.57
${ m TiO_2}$								
	Γ	1.91	4.31	-	2.40	-	25	2.44
MAE		0.30	0.97					0.06
$\mathrm{MARE}(\%)$		5.8	22.1					1.1

^a Ref. [36]

electrons. The frequency integrals in Eqs. (3) and (6) were converged on an adapted grid of 8 frequency points. The RPA KS gap of the rutile phase of ${\rm TiO_2}$ was converged within 0.05 eV using 360 eigenvalues and a $3\times3\times3$ k-point grid.

For the RPA/ G_0W_0 band gap calculations at experimental lattice constants, we used the YAMBO code with full frequency integration [79, 80]. Gaps were converged with respect to the number of bands, frequency points and G-vector cutoff for the response function. We used a k-point grid of $6\times6\times6$, except in the case of TiO₂ for which we used a $4\times4\times4$ grid. We needed 1000-1500 frequency points and a response function cutoff within 15-26 Ry. The number of bands included were: 160 for C, 110 for Si, 160 for BN, 350 for LiF, 520 for MgO, and 2000 for TiO₂. The setup for TiO₂ is very close to the one

used in a recent precision benchmark calculation [81].

B. RPA KS potential

In Table I, we present KS band gaps obtained with PBE, EXX, RPA, and the variationally optimized OEP $\alpha_{\rm RPA}$ hybrid functional. The RPA and EXX results are compared to the results obtained with the PAW method, as implemented in the VASP code [37]. For both EXX and RPA, we find good agreement between the two implementations. Differences are less than 0.1 eV, and, in most cases, below 0.05 eV. Variations of similar order are already found at the PBE level (not shown in the table), suggesting that the differences are mostly due to different treatments of the core electrons. We note that

^b Results for C, Si, BN and MgO are from Ref. [37]. Results for LiF are from Ref. [35] (*) and Ref. [36] (†).

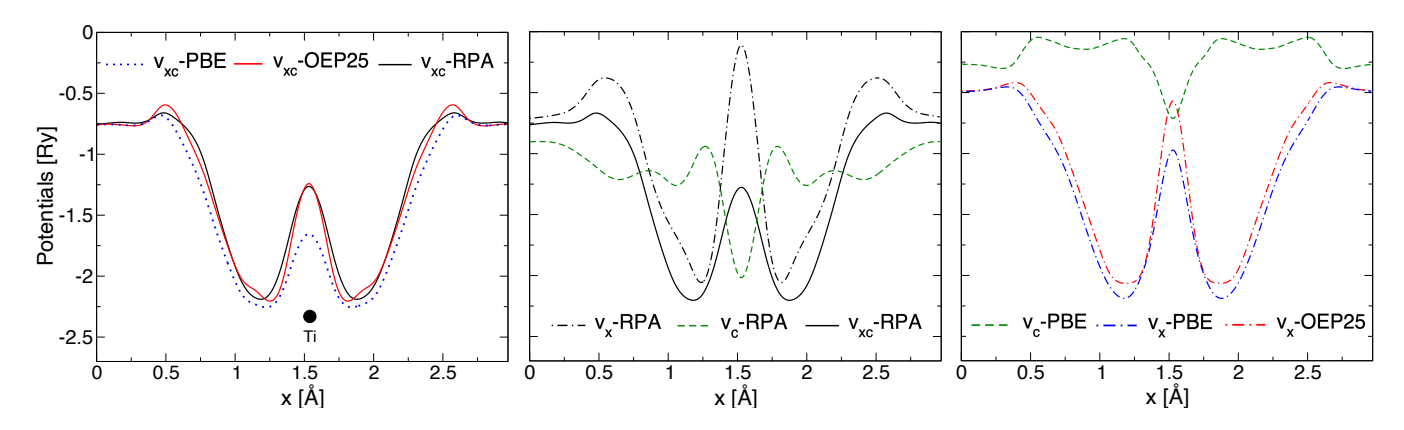


Figure 3. KS potentials of TiO₂ along the [001] direction. Left panel: xc potentials calculated with PBE, RPA, and the optimized hybrid functional OEP25. The position of the Ti atom is marked with a black dot. Middle panel: RPA xc potential decomposed into its exchange and correlation components. Right panel: PBE correlation potential and PBE and OEP25 exchange potentials.

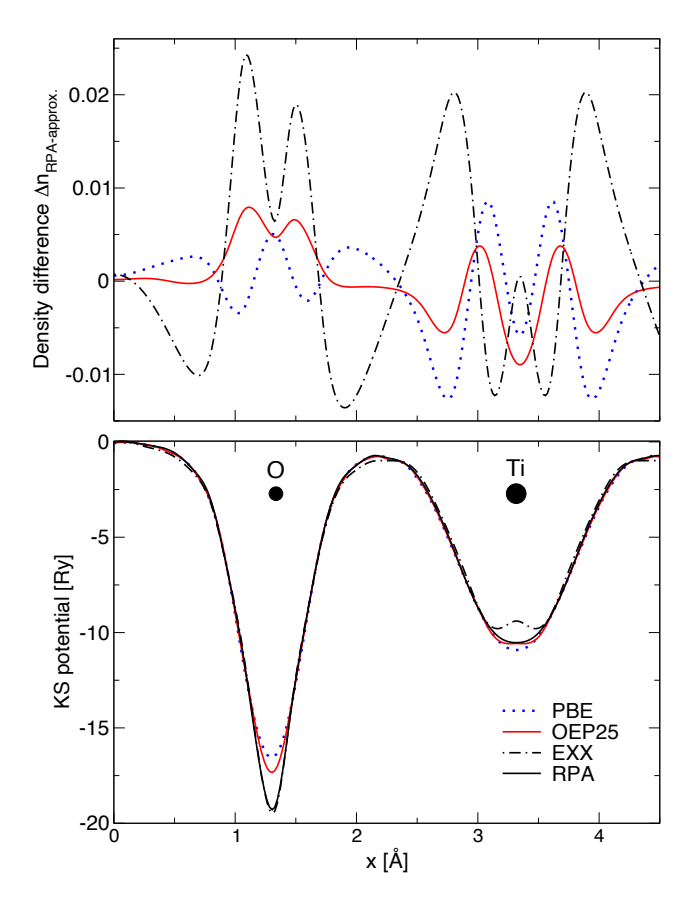


Figure 4. KS densities and potential of TiO_2 along the [110] direction. Top panel: density difference $\Delta n_{\text{RPA-approx.}}$, where "approx." corresponds to PBE, EXX, or OEP25. Bottom panel: total KS potential of TiO_2 . The positions of the O and Ti atoms are marked with black dots.

the two RPA reference values for LiF were obtained either by evaluating the screened interaction with EXX orbitals in combination with the plasmon pole approximation (*) [35], or by employing the quasiparticle approximation to the GW self-energy (†) [36]. The latter was later shown to significantly affect the gaps [37]. The effect of the plasmon pole approximation remains unclear.

We find that self-consistency lowers the RPA energy with respect to the use of PBE, EXX, and OEP α starting points. By restricting the RPA variational freedom to KS potentials from OEP α , we find, in all cases studied, a minimum at a given $\alpha = \alpha_{\rm RPA}$. This is demonstrated in Fig. 1, where we plot the RPA total energy for C, Si and BN as a function of α . The value of $\alpha_{\rm RPA}$, as presented in Tab. I, is, as expected, system dependent.

By looking at the mean absolute error (MAE) and the mean absolute relative error (MARE(%)) of the KS gaps in PBE, EXX and OEP α_{RPA} with respect to RPA, we see that PBE is closer to RPA (MAE: 0.30 eV and MARE%: 5.8%) than EXX (MAE: 0.97 eV and MARE%: 22.1%). We also see that RPA and $OEP\alpha_{RPA}$ agree rather well (MAE: 0.06 eV and MARE%: 1.1%), suggesting that the hybrid potential is able to mimic the RPA potential, at least in the set of solids studied here. This validates the α -optimization procedure, which we emphasize only indirectly optimizes the potentials via the total energy. The largest difference is found for C and LiF, where the gaps differ by around 0.1 eV. Focusing on C, we found that it is possible to get a better agreement with RPA by increasing the fraction of exact exchange from 17% to 34%. The latter value gives the gaps $\Gamma - \Gamma = 5.74$ eV, $\Gamma - L = 8.61 \text{ eV}$ and $\Gamma - X = 4.86 \text{ eV}$, which almost coincide with the RPA gaps. In order to investigate why the α -optimization does not find this seemingly better value of α , we have analyzed the corresponding KS potentials and densities. The top and middle panels of Fig. 2 show the total and the xc part of the C KS potential along the [111] direction. The density difference with respect to the RPA density is shown in the bottom panel of the same figure. Visually, it appears difficult to reproduce the full spatial structure of the RPA potential with OEP α . The OEP34 looks somewhat better than OEP17 in the C-C bond region but worsens towards the interstitial region.

Looking at density differences is somewhat more informative. The optimized OEP17 functional overall better reproduces the RPA density than OEP34, especially the amount of charge density localized in the vicinity of the C-C bond. The OEP34 instead over-localizes the density, an effect that only gets stronger the larger the fraction of exact exchange. The OEP α potential thus appears not flexible enough to fully reproduce both gaps and densities using the same value of α .

Let us now focus on ${\rm TiO}_2$, a system relatively sensitive to a fraction of exact exchange in the PBE functional. Looking at the $\Gamma - \Gamma$ gap, we find very good agreement between RPA and OEP α_{RPA} . The xc potentials are plotted in Fig. 3 along the [001] direction, i.e., along an axis that crosses Ti-atoms only. In the left panel, the RPA xc potential is compared to the OEP25 and PBE xc potentials. PBE clearly predicts a wider potential well and underestimates the height of the barrier at the center of the atom. By including 25% of exact exchange as within the optimized OEP25, it is possible to reproduce most of the features of the RPA potential. The well width and the height of the barrier now almost coincide. A difference is seen at the edges of the well where OEP25 gives a sharper step-structure, as opposed to the narrowing of the well observed in RPA.

In order to gain further insights, we have decomposed the xc potentials into their exchange and correlation components, shown in the middle and right panels of Fig. 3. The correlation potentials in RPA and PBE are seen to be rather different. Except for a dip at the position of the atom, the PBE correlation potential is almost inverted as compared to the RPA correlation potential. This effect appears similar to what has already been observed in atoms [28]. The PBE correlation potential thus simulates features of the exact exchange potential that are underestimated by the PBE exchange potential, leading to a compensation of errors between exchange and correlation components.

In Fig. 4, we have plotted the total KS potential of TiO_2 along a direction that crosses both O and Ti atoms. In the top panel, the density difference with respect to RPA is plotted along the same path for PBE, EXX, and OEP25. As expected, the density difference is minimized with the optimized OEP25 functional, especially in the vicinity of the Ti atom and in-between the O and Ti atoms.

C. Lattice constants

To further evaluate the performance of the RPA optimized hybrid functionals, we have calculated lattice constants for the set of solids studied above. The results, presented in Tab. III, are compared to the RPA results obtained in the present work and to those within the PAW framework [82]. PBE and experimental values are also indicated. The latter, extracted from Ref. [82], are corrected for zero-point anharmonic expansion effects in

all cases except TiO₂. Since self-consistency was found to play an insignificant role in diamond, the RPA lattice constants are obtained by evaluating the RPA energy on top of PBE orbitals. For the self-consistent hybrid functional calculations, we used the nonlocal hybrid potential. The results are therefore denoted PBE0 $\alpha_{\rm RPA}$. Using the local OEP $\alpha_{\rm RPA}$ hybrid potential did not change the results.

The lattice constant is a property obtained from the first derivative of the energy, which is directly determined by the electronic density. By comparing PBE0 $\alpha_{\rm RPA}$ and RPA lattice constants, we therefore get a measure of how similar the densities are. The results are illustrated in Fig. 5, where the relative (%) error with respect to corrected experimental results is plotted for all approximations and solids. For Si, LiF and MgO, a fraction of exact exchange largely improves the PBE lattice constants. At the same time, the PBE0 α_{RPA} results agree well with RPA. Good α values are also found for C and BN, producing lattice constants in better agreement with experimental results than the underlying RPA functional, which, in these cases, gives results very close to PBE. The performance of the optimized hybrid functionals is thus either similar or better than RPA.

Overall, RPA significantly improves upon PBE, consistent with similar results for a larger set of solids in Ref. [82]. We find good agreement between the RPA lattice constants obtained in this work and those obtained using the PAW method for C, LiF and MgO [82]. In contrast, for Si we see a difference of almost 0.02 Å, with an underestimation in the present work. However, if we compare to a previous similar calculation using a norm-conserving pseudopotential, we find our result to be overestimated by 0.03 Å [61]. There is thus a span of 5.38Å-5.43Å in the published results of the RPA lattice constant of Si. Our result using the ONCV pseudo potential is somewhere in-between previous calculations. This suggests that the results for Si are very sensitive to the construction of the pseudopotential. Further investigations are needed to clear up this issue.

D. RPA band gaps

In Table III, we present quasi-particle band gaps evaluated within the G_0W_0 approximation. Since we have omitted the renormalization factor in all calculations, we will from now on refer to them as RPA gaps. The difference is relevant since the renormalisation factor reduces the values of the gaps by around 0.5 eV. The starting-point dependence is studied by calculating the RPA gaps starting from PBE, OEP $\alpha_{\rm RPA}$, and RPA KS potentials. In the following, we will indicate the starting-point approximation with the standard notation "@".

A new optimal fraction of exact exchange within OEP α was then obtained by the approach detailed in Sec. II B. We find that this gap-optimized, $\alpha_{\rm opt}$, in general, is different from the variationally optimized, $\alpha_{\rm RPA}$, obtained

Table II. Lattice constants (Å) obtained with PBE, RPA, and PBE0 α_{RPA} (see Table I for α^{RPA}). Results are compared to the reference RPA and experimental results corrected for zeropoint anharmonic expansion effects published in Ref. [82]. The experimental extrapolated T=0 K results for the lattice constants a and c of rutile TiO₂ are taken from Ref. [83]. The relative (%) error for each approximation with respect to experiment is illustrated in Fig. 5.

Solid	PBE	$PBE0\alpha_{RPA}$	RPA	RPA lit.	Exp.
С	3.567	3.552	3.567	3.572	3.553
Si	5.479	5.435	5.414	5.432	5.421
BN	3.621	3.599	3.617	-	3.592
LiF	4.062	4.007	3.993	3.998	3.972
$_{\rm MgO}$	4.255	4.208	4.211	4.225	4.189
$TiO_2(a)$	4.640	4.586	4.596	-	4.586
$\mathrm{TiO}_{2}(c)$	2.971	2.945	2.956	-	2.952

above. The PBE0 $\alpha_{\rm RPA}$ functional tends to underestimate the gaps except for Si and TiO₂, where the gap is overestimated. It is well-known that the PBE0 α gaps are strongly dependent on α . Indeed, if we look at diamond, we see that changing α from 17% ($\alpha_{\rm RPA}$) to 25% ($\alpha_{\rm opt}$) increases the PBE0 α gap by about 0.7 eV. In LiF, a change from 26% ($\alpha_{\rm RPA}$) to 46% ($\alpha_{\rm opt}$) increases the gap by about 2.4 eV. Given these differences between $\alpha_{\rm RPA}$ and $\alpha_{\rm opt}$, we conclude that it is difficult to achieve high accuracy on the gap and the density simultaneously.

For C, Si, and BN, the RPA gaps have a very weak starting-point dependence. In the polar solids LiF and MgO, we see more significant changes, of the order of $0.3~\rm eV$ between the PBE and RPA starting-points. TiO₂ has the strongest starting-point dependence. The gap changes as much as $0.5~\rm eV$ going from PBE to RPA KS potentials. Looking at the relative difference, the change

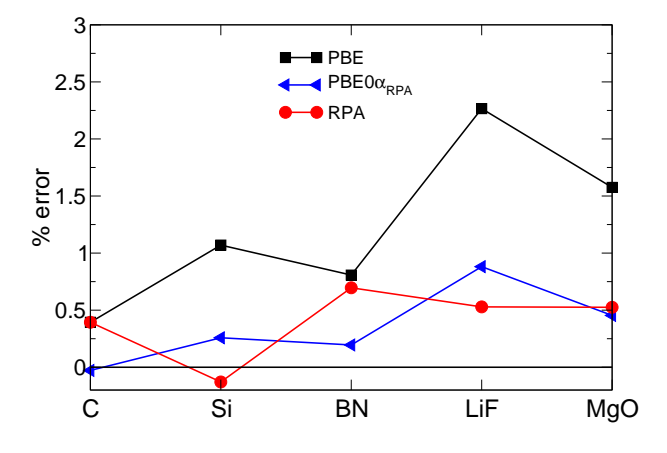


Figure 5. The relative (%) error with respect to corrected experimental results for PBE, RPA, and the optimized hybrid functional PBE0 $\alpha_{\rm RPA}$ (see Table I for the values of $\alpha^{\rm RPA}$).

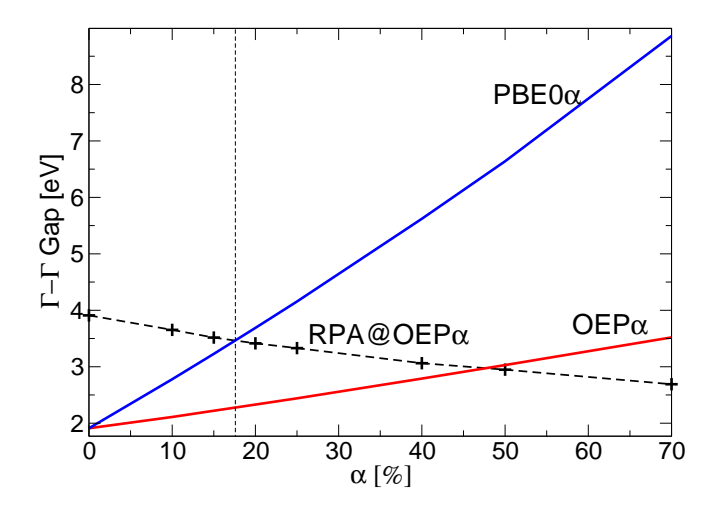


Figure 6. $\Gamma - \Gamma$ gap of TiO₂ for PBE0 α , OEP α , and RPA@OEP α , plotted as a function of α . The crossing of PBE0 α and RPA@OEP α corresponds to $\alpha_{\rm opt}$ (marked with a dashed vertical line).

is as large as 15% in TiO₂ but only 2-3% in MgO and LiF. The starting-point dependence is also unusual in TiO₂. While in most solids the RPA gap increases with larger fractions of exact-exchange, we see the opposite trend in TiO₂ (see Fig. 6). The larger the gap in OEP α the smaller the RPA gap. With an OEP70 starting point, the gap is as small as 2.7 eV. Similar observations were made for TiSe₂, TiS₂ and ScN in Ref. [53] and in TiO₂ using an LDA+U starting point [50]. With such a strong dependency on the starting point, the only meaningful result is the one obtained with the RPA potential. Here, we see that OEP α _{opt} can provide a similar value.

Next, we compare the RPA gaps to the experimentally measured gaps. In most cases the RPA overestimates experimental gap. On the other hand, zero-point renormalization due to electron-phonon interactions have recently been shown to reduce the calculated gaps substantially. In Ref. [84] the corrections we determined to be -0.323 eV for C, -0.058 eV for Si, -0.400 eV for BN, -1.231 eV for LiF, -0.533 eV for MgO, and -0.349 eV for TiO₂. Adding these values to the RPA gaps brings them in better agreement with experiment. MgO and LiF remains, however, underestimated, suggesting the need for vertex corrections.

IV. CONCLUSIONS

In this work, we have calculated RPA KS potentials for a set of solids by extending a plane-wave implementation previously applied to molecules. The key feature of this implementation is the eigendecomposition of the KS response function together with the use of DFPT, which eliminates the need to generate unoccupied KS states, both for the energy and the gradient. The computational cost of evaluating the gradient+energy is roughly

Table III. Band gaps (eV) of C, Si, BN, LiF, MgO, and rutile TiO₂, between Γ and different k-points. The RPA gaps (equivalent to G_0W_0 gaps without the renormalization factor) are obtained with a KS starting point from PBE, RPA, OEP α_{RPA} and OEP α_{opt} . The corresponding PBE0 α results and the α_{opt} (%) are also given. The α_{RPA} values are given in Table I.

Solid	k	RPA@PBE	RPA@RPA	$PBE0\alpha_{RPA}$	RPA@OEP α_{RPA}	$\alpha_{ m opt}$	$PBE0\alpha_{opt}$	RPA@OEP α_{opt}	Exp.
С									
	Γ	7.67	7.73	7.04	7.69	25	7.72	7.71	7.1^{a}
	\mathbf{L}	10.63	10.69	10.06	10.65		10.80	10.67	
	X	6.25	6.30	6.11	6.29		6.72	6.32	
Si									
	Γ	3.39	3.39	4.18	3.43	16	3.45	3.43	$3.05^{\rm b}$
	L	2.36	2.35	3.08	2.39		2.37	2.39	
	X	1.46	1.40	2.11	1.48		1.47	1.49	$1.25^{\rm b}$
BN									
	Γ	11.50	11.50	10.98	11.54	25	11.28	11.53	
	L	12.39	12.41	12.35	12.44		12.54	12.43	
	X	6.56	6.57	6.36	6.62		6.61	6.61	$6.36^{\rm c}$
LiF									
	Γ	14.55	14.85	12.41	14.74	46	14.86	14.85	$14.20^{\rm d}$
	\mathbf{L}	16.25	16.54	14.12	16.42		16.58	16.53	
	X	21.23	21.52	18.49	21.44		21.20	21.56	
$_{\mathrm{MgO}}$									
	Γ	7.72	7.98	7.10	7.85	32	7.90	7.87	$7.83^{\rm e}$
	L	11.18	11.37	10.37	11.28		11.20	11.30	
	X	12.17	12.98	11.53	12.27		12.33	12.28	
${\rm TiO_2}$									
	Γ	3.91	3.40	4.16	3.33	18	3.50	3.46	3.0 ^f

^a Ref. [85].

twice the cost of evaluating the energy alone. We found a smooth convergence of the RPA potential in all cases studied. KS band gaps were converged within 0.02 eV using a small number of eigenvalues (approximately 5 times the number of electrons). We also found good agreement with first calculations that used the PAW method.

The RPA total energy was then studied with respect to different starting points. In all solids, self-consistent RPA was lower in energy as compared to RPA with a PBE or $\text{OEP}\alpha$ starting point. By restricting the domain of KS potentials to $\text{OEP}\alpha$ hybrid potentials, a variational scheme for optimizing α was devised. We showed that the resulting hybrid potential produced a KS band structure very close to the RPA band structure, and that the corresponding lattice constant was of similar quality as the RPA lattice constant. This method thus provides a reliable tool for generating predictive system-optimized

hybrid functionals. Such hybrid functionals can be used to compute properties such as geometries and phonon frequencies, for which RPA may be computationally too demanding.

The starting-point dependence of the RPA band gaps (equal to the G_0W_0 band gaps without the renormalization factor) were then studied together with an alternative approach for optimizing the fraction of exact exchange of the PBE0 functional. For most solids studied here we found a relatively weak dependency on the starting point. An exception is TiO_2 , where we found variations as large as 1.5 eV (about 40% of the gap), depending on the fraction of exact exchange in the $\text{OEP}\alpha$ starting point. Surprisingly, the larger the α the smaller the RPA gap, similar to what has been found in TiSe_2 , TiS_2 , and ScN. In general, the optimization of α via the RPA gap results in values for α different from those ob-

^b Ref. [86].

^c Ref. [87].

d Ref. [88].

^e Ref. [89].

f Ref. [90].

tained after variational optimization. This demonstrates that, in many cases, it is not possible to get accurate gaps and structures using the same fraction of exact exchange. Which approach is more suitable depends on the property to be studied. It should be noted, however, that the methodology presented here is not limited to PBE0, but may be applied also to more flexible hybrid functionals with more than a single parameter to be optimized. Finally, we expect further improvements of the values for α using the more accurate RPA + exchange (RPAx) functional [68, 75]. Such investigations are left for future work.

APPENDIX

The functional derivative of χ_s with respect to V_s is here given in terms of KS orbitals and eigenvalues

$$\frac{\delta \chi_{s}(i\omega)}{\delta V_{s}(\mathbf{r})} =$$

$$= \sum_{kk'p} \left\{ -\frac{n_{k'}(1-n_{k})(1-n_{p})}{(\varepsilon_{p}-\varepsilon_{k'})(\pm i\omega - (\varepsilon_{k}-\varepsilon_{k'}))} - \frac{n_{p}(1-n_{k'})(1-n_{k})}{(\varepsilon_{k'}-\varepsilon_{p})(\pm i\omega - (\varepsilon_{k}-\varepsilon_{p}))} + \frac{n_{k}(1-n_{p})n_{k'}}{(\varepsilon_{p}-\varepsilon_{k'})(\pm i\omega - (\varepsilon_{p}-\varepsilon_{k}))} + \frac{n_{k}(1-n_{k'})n_{p}}{(\varepsilon_{k'}-\varepsilon_{p})(\pm i\omega - (\varepsilon_{k'}-\varepsilon_{k}))} - \frac{n_{k'}(1-n_{k})n_{p}}{(\pm i\omega - (\varepsilon_{k}-\varepsilon_{k'}))(\pm i\omega - (\varepsilon_{k}-\varepsilon_{p}))} + \frac{n_{k}(1-n_{k'})(1-n_{p})}{(\pm i\omega - (\varepsilon_{k'}-\varepsilon_{k}))(\pm i\omega - (\varepsilon_{p}-\varepsilon_{k}))} \right\} \times \varphi_{p}(\mathbf{r})\varphi_{k'}^{*}(\mathbf{r})\varphi_{k}(\mathbf{r}_{1})\varphi_{p}^{*}(\mathbf{r}_{1})\varphi_{k}^{*}(\mathbf{r}_{2})\varphi_{k'}(\mathbf{r}_{2}) \tag{16}$$

- J. Harl and G. Kresse, Cohesive energy curves for noble gas solids calculated by adiabatic connection fluctuationdissipation theory, Phys. Rev. B 77, 045136 (2008).
- [2] M. Rohlfing and T. Bredow, Binding energy of adsorbates on a noble-metal surface: Exchange and correlation effects, Phys. Rev. Lett. 101, 266106 (2008).
- [3] D. Lu, Y. Li, D. Rocca, and G. Galli, Ab initio calculation of van der waals bonded molecular crystals, Phys. Rev. Lett. 102, 206411 (2009).
- [4] X. Ren, P. Rinke, and M. Scheffler, Exploring the random phase approximation: Application to co adsorbed on cu(111), Phys. Rev. B 80, 045402 (2009).
- [5] J. Harl and G. Kresse, Accurate bulk properties from approximate many-body techniques, Phys. Rev. Lett. 103, 056401 (2009).
- [6] L. Schimka, J. Harl, A. Stroppa, A. Grüneis, M. Marsman, F. Mittendorfer, and G. Kresse, Accurate surface and adsorption energies from many-body perturbation theory, Nature materials 9, 741 (2010).
- [7] F. Mittendorfer, A. Garhofer, J. Redinger, J. Klimeš, J. Harl, and G. Kresse, Graphene on ni(111): Strong interaction and weak adsorption, Phys. Rev. B 84, 201401 (2011).
- [8] T. Olsen, J. Yan, J. J. Mortensen, and K. S. Thygesen, Dispersive and covalent interactions between graphene and metal surfaces from the random phase approximation, Phys. Rev. Lett. 107, 156401 (2011).
- [9] H.-J. Kim, A. Tkatchenko, J.-H. Cho, and M. Scheffler, Benzene adsorbed on si(001): The role of electron correlation and finite temperature, Phys. Rev. B 85, 041403 (2012).

- [10] X. Ren, P. Rinke, C. Joas, and M. Scheffler, Randomphase approximation and its applications in computational chemistry and materials science, Journal of Materials Science 47, 7447 (2012).
- [11] H. Eshuis, J. E. Bates, and F. Furche, Electron correlation methods based on the random phase approximation, Theoretical Chemistry Accounts 131, 1084 (2012).
- [12] B. Ramberger, T. Schäfer, and G. Kresse, Analytic interatomic forces in the random phase approximation, Phys. Rev. Lett. 118, 106403 (2017).
- [13] J. Klimeš and D. P. Tew, Efficient and accurate description of adsorption in zeolites, The Journal of Chemical Physics 151, 234108 (2019).
- [14] C. Cazorla and T. Gould, Polymorphism of bulk boron nitride, Science Advances 5, eaau5832 (2019).
- [15] F. Jia, G. Kresse, C. Franchini, P. Liu, J. Wang, A. Stroppa, and W. Ren, Cubic and tetragonal perovskites from the random phase approximation, Phys. Rev. Mater. 3, 103801 (2019).
- [16] C. Sheldon, J. Paier, and J. Sauer, Adsorption of ch4 on the pt(111) surface: Random phase approximation compared to density functional theory, The Journal of Chemical Physics 155, 174702 (2021).
- [17] F. Furche, Molecular tests of the random phase approximation to the exchange-correlation energy functional, Phys. Rev. B 64, 195120 (2001).
- [18] M. Fuchs, Y.-M. Niquet, X. Gonze, and K. Burke, Describing static correlation in bond dissociation by Kohn-Sham density functional theory, The Journal of Chemical Physics 122, 094116 (2005).

- [19] A. Heßelmann and A. Görling, Correct description of the bond dissociation limit without breaking spin symmetry by a random-phase-approximation correlation functional, Phys. Rev. Lett. 106, 093001 (2011).
- [20] M. Hellgren, D. R. Rohr, and E. K. U. Gross, Correlation potentials for molecular bond dissociation within the selfconsistent random phase approximation, The Journal of Chemical Physics 136, 034106 (2012).
- [21] F. Caruso, D. R. Rohr, M. Hellgren, X. Ren, P. Rinke, A. Rubio, and M. Scheffler, Bond breaking and bond formation: How electron correlation is captured in manybody perturbation theory and density-functional theory, Phys. Rev. Lett. 110, 146403 (2013).
- [22] M. Hellgren, F. Caruso, D. R. Rohr, X. Ren, A. Rubio, M. Scheffler, and P. Rinke, Static correlation and electron localization in molecular dimers from the selfconsistent rpa and gw approximation, Phys. Rev. B 91, 165110 (2015).
- [23] M. Hellgren and U. von Barth, Correlation potential in density functional theory at the gwa level: Spherical atoms, Phys. Rev. B 76, 075107 (2007).
- [24] N. L. Nguyen, N. Colonna, and S. de Gironcoli, Ab initio self-consistent total-energy calculations within the exx/rpa formalism, Phys. Rev. B 90, 045138 (2014).
- [25] M. Hellgren and T. Gould, Strong correlation and charge localization in kohn–sham theories with fractional orbital occupations, Journal of chemical theory and computation 15, 4907 (2019).
- [26] E. Trushin, S. Fauser, A. Mölkner, J. Erhard, and A. Görling, Accurate correlation potentials from the selfconsistent random phase approximation, Phys. Rev. Lett. 134, 016402 (2025).
- [27] C. J. Umrigar and X. Gonze, Accurate exchangecorrelation potentials and total-energy components for the helium isoelectronic series, Phys. Rev. A 50, 3827 (1994).
- [28] H. Jiang and E. Engel, Second-order kohn-sham perturbation theory: Correlation potential for atoms in a cavity, The Journal of Chemical Physics 123, 224102 (2005).
- [29] Y. M. Niquet, M. Fuchs, and X. Gonze, Exchangecorrelation potentials in the adiabatic connection fluctuation-dissipation framework, Phys. Rev. A 68, 032507 (2003).
- [30] O. V. Gritsenko and E. J. Baerends, Effect of molecular dissociation on the exchange-correlation kohn-sham potential, Phys. Rev. A 54, 1957 (1996).
- [31] S. Kümmel and L. Kronik, Orbital-dependent density functionals: Theory and applications, Rev. Mod. Phys. 80, 3 (2008).
- [32] F. G. Eich and M. Hellgren, Derivative discontinuity and exchange-correlation potential of meta-ggas in densityfunctional theory, The Journal of Chemical Physics 141, 224107 (2014).
- [33] Z.-h. Yang, H. Peng, J. Sun, and J. P. Perdew, More realistic band gaps from meta-generalized gradient approximations: Only in a generalized kohn-sham scheme, Phys. Rev. B 93, 205205 (2016).
- [34] R. W. Godby, M. Schlüter, and L. J. Sham, Trends in self-energy operators and their corresponding exchangecorrelation potentials, Phys. Rev. B 36, 6497 (1987).
- [35] M. Grüning, A. Marini, and A. Rubio, Density functionals from many-body perturbation theory: The band gap for semiconductors and insulators, The Journal of Chemical Physics 124, 154108 (2006).

- [36] J. Klimes and G. Kresse, Kohn-sham band gaps and potentials of solids from the optimised effective potential method within the random phase approximation, The Journal of Chemical Physics 140, 054516 (2014).
- [37] S. Riemelmoser, M. Kaltak, and G. Kresse, Optimized effective potentials from the random-phase approximation: Accuracy of the quasiparticle approximation, The Journal of Chemical Physics 154, 154103 (2021).
- [38] J. P. Perdew, R. G. Parr, M. Levy, and J. L. Balduz, Density-functional theory for fractional particle number: Derivative discontinuities of the energy, Phys. Rev. Lett. 49, 1691 (1982).
- [39] W. Yang, A. J. Cohen, and P. Mori-Sánchez, Derivative discontinuity, bandgap and lowest unoccupied molecular orbital in density functional theory, The Journal of Chemical Physics 136, 204111 (2012).
- [40] W. Kohn and L. J. Sham, Self-Consistent Equations Including Exchange and Correlation Effects, Physical Review 140, A1133 (1965).
- [41] C.-O. Almbladh and U. von Barth, Exact results for the charge and spin densities, exchange-correlation potentials, and density-functional eigenvalues, Phys. Rev. B 31, 3231 (1985).
- [42] M. Petersilka, U. J. Gossmann, and E. K. U. Gross, Excitation energies from time-dependent density-functional theory, Phys. Rev. Lett. 76, 1212 (1996).
- [43] M. A. L. Marques, C. A. Ullrich, F. Nogueira, A. Rubio, K. Burke, and E. K. U. Gross, *Time-Dependent Density Functional Theory*, Vol. 706 (Springer, Berlin, Heidelberg, 2006).
- [44] M. S. Hybertsen and S. G. Louie, Electron correlation in semiconductors and insulators: Band gaps and quasiparticle energies, Phys. Rev. B 34, 5390 (1986).
- [45] F. Aryasetiawan and O. Gunnarsson, The gw method, Reports on Progress in Physics **61**, 237 (1998).
- [46] L. Reining, The gw approximation: content, successes and limitations, WIREs Computational Molecular Science 8, e1344 (2018).
- [47] Y. M. Niquet and X. Gonze, Band-gap energy in the random-phase approximation to density-functional theory, Phys. Rev. B 70, 245115 (2004).
- [48] M. Shishkin and G. Kresse, Self-consistent gw calculations for semiconductors and insulators, Phys. Rev. B 75, 235102 (2007).
- [49] M. van Schilfgaarde, T. Kotani, and S. Faleev, Quasi-particle self-consistent gw theory, Phys. Rev. Lett. **96**, 226402 (2006).
- [50] C. E. Patrick and F. Giustino, Gw quasiparticle bandgaps of anatase tio2 starting from dft+ u, Journal of Physics: Condensed Matter 24, 202201 (2012).
- [51] V. Atalla, M. Yoon, F. Caruso, P. Rinke, and M. Scheffler, Hybrid density functional theory meets quasiparticle calculations: A consistent electronic structure approach, Phys. Rev. B 88, 165122 (2013).
- [52] C. Mitra, Extracting the hybrid functional mixing parameter from a gw quasiparticle approach, physica status solidi (b) **250**, 1449 (2013).
- [53] M. Hellgren, L. Baguet, M. Calandra, F. Mauri, and L. Wirtz, Electronic structure of tise₂ from a quasi-self-consistent G_0W_0 approach, Phys. Rev. B **103**, 075101 (2021).
- [54] R. T. Sharp and G. K. Horton, A Variational Approach to the Unipotential Many-Electron Problem, Physical Review 90, 317 (1953).

- [55] J. D. Talman and W. F. Shadwick, Optimized effective atomic central potential, Physical Review A 14, 36 (1976).
- [56] M. Städele, M. Moukara, J. A. Majewski, P. Vogl, and A. Görling, Exact exchange kohn-sham formalism applied to semiconductors, Phys. Rev. B 59, 10031 (1999).
- [57] D. Contant, M. Casula, and M. Hellgren, Assessing many-body methods on the potential energy surface of the (h2)2 hydrogen dimer, The Journal of Chemical Physics 161, 184107 (2024).
- [58] M. Hellgren and U. von Barth, Exact-exchange kernel of time-dependent density functional theory: Frequency dependence and photoabsorption spectra of atoms, The Journal of Chemical Physics 131, 044110 (2009).
- [59] A. Makmal, S. Kümmel, and L. Kronik, Fully numerical all-electron solutions of the optimized effective potential equation for diatomic molecules, Journal of Chemical Theory and Computation 5, 1731 (2009), pMID: 26609998.
- [60] E. Trushin and A. Görling, Numerically stable optimized effective potential method with standard gaussian basis sets, The Journal of Chemical Physics 155, 054109 (2021).
- [61] H.-V. Nguyen and S. de Gironcoli, Efficient calculation of exact exchange and RPA correlation energies in the adiabatic-connection fluctuation-dissipation theory, Physical Review B 79, 205114 (2009).
- [62] A. Klein, Perturbation theory for an infinite medium of fermions. ii, Phys. Rev. 121, 950 (1961).
- [63] A. L. Fetter and J. D. Walecka, Quantum Theory of Many-Particle Systems, 2nd ed. (Dover Publ., New York, 2003).
- [64] J. P. Perdew, K. Burke, and M. Ernzerhof, Generalized Gradient Approximation Made Simple, Physical Review Letters 77, 3865 (1996).
- [65] J. P. Perdew, K. Burke, and M. Ernzerhof, Generalized Gradient Approximation Made Simple [Phys. Rev. Lett. 77, 3865 (1996)], Physical Review Letters 78, 1396 (1997).
- [66] J. B. Krieger, Y. Li, and G. J. Iafrate, Construction and application of an accurate local spin-polarized kohn-sham potential with integer discontinuity: Exchange-only theory, Phys. Rev. A 45, 101 (1992).
- [67] S. Kümmel and J. P. Perdew, Optimized effective potential made simple: Orbital functionals, orbital shifts, and the exact Kohn-Sham exchange potential, Physical Review B 68, 035103 (2003).
- [68] M. Hellgren and U. von Barh, Correlation energy functional and potential from time-dependent exact-exchange theory, The Journal of Chemical Physics 132, 044101 (2010).
- [69] P. Giannozzi, O. Andreussi, T. Brumme, O. Bunau, M. Buongiorno Nardelli, M. Calandra, R. Car, C. Cavazzoni, D. Ceresoli, M. Cococcioni, N. Colonna, I. Carnimeo, A. Dal Corso, S. de Gironcoli, P. Delugas, R. A. DiStasio, A. Ferretti, A. Floris, G. Fratesi, G. Fugallo, R. Gebauer, U. Gerstmann, F. Giustino, T. Gorni, J. Jia, M. Kawamura, H.-Y. Ko, A. Kokalj, E. Kucukbenli, M. Lazzeri, M. Marsili, N. Marzari, F. Mauri, N. L. Nguyen, H.-V. Nguyen, A. Otero-de-la Roza, L. Paulatto, S. Poncé, D. Rocca, R. Sabatini, B. Santra, M. Schlipf, A. P. Seitsonen, A. Smogunov, I. Timrov, T. Thonhauser, P. Umari, N. Vast, X. Wu, and S. Baroni, Advanced capabilities for materials modelling with Quan-

- tum ESPRESSO, Journal of Physics: Condensed Matter **29**, 465901 (2017).
- [70] S. Baroni, P. Giannozzi, and A. Testa, Green's-function approach to linear response in solids, Phys. Rev. Lett. 58, 1861 (1987).
- [71] S. Baroni, S. de Gironcoli, A. Dal Corso, and P. Giannozzi, Phonons and related crystal properties from density-functional perturbation theory, Rev. Mod. Phys. 73, 515 (2001).
- [72] S. Kümmel and J. P. Perdew, Simple Iterative Construction of the Optimized Effective Potential for Orbital Functionals, Including Exact Exchange, Physical Review Letters 90, 043004 (2003).
- [73] N. E. Dahlen, R. van Leeuwen, and U. von Barth, Variational energy functionals of the green function and of the density tested on molecules, Phys. Rev. A 73, 012511 (2006).
- [74] C. Adamo and V. Barone, Toward reliable density functional methods without adjustable parameters: The PBE0 model, The Journal of Chemical Physics 110, 6158 (1999).
- [75] M. Hellgren and L. Baguet, Random phase approximation with exchange for an accurate description of crystalline polymorphism, Physical Review Research 3, 033263 (2021).
- [76] M. Hellgren, D. Contant, T. Pitts, and M. Casula, Highpressure II-III phase transition in solid hydrogen: Insights from state-of-the-art ab initio calculations, Physical Review Research 4, L042009 (2022).
- [77] M. Hellgren and E. K. U. Gross, Discontinuities of the exchange-correlation kernel and charge-transfer excitations in time-dependent density-functional theory, Phys. Rev. A 85, 022514 (2012).
- [78] D. R. Hamann, Optimized norm-conserving Vanderbilt pseudopotentials. Physical Review B 88, 085117 (2013).
- [79] A. Marini, C. Hogan, M. Grüning, and D. Varsano, yambo: An ab initio tool for excited state calculations, Computer Physics Communications 180, 1392 (2009).
- [80] D. Sangalli, A. Ferretti, H. Miranda, C. Attaccalite, I. Marri, E. Cannuccia, P. Melo, M. Marsili, F. Paleari, A. Marrazzo, et al., Many-body perturbation theory calculations using the yambo code, Journal of Physics: Condensed Matter 31, 325902 (2019).
- [81] M. Azizi, F. A. Delesma, M. Giantomassi, D. Zavickis, M. Kuisma, K. Thyghesen, D. Golze, A. Buccheri, M.-Y. Zhang, P. Rinke, C. Draxl, A. Gulans, and X. Gonze, Precision benchmarks for solids: G0w0 calculations with different basis sets, arXiv preprint arXiv:2411.19701 (2024).
- [82] J. Harl, L. Schimka, and G. Kresse, Assessing the quality of the random phase approximation for lattice constants and atomization energies of solids, Phys. Rev. B 81, 115126 (2010).
- [83] D. R. Hummer, P. J. Heaney, and J. E. Post, Thermal expansion of anatase and rutile between 300 and 575 k using synchrotron powder x-ray diffraction, Powder Diffraction 22, 352–357 (2007).
- [84] M. Engel, H. Miranda, L. Chaput, A. Togo, C. Verdi, M. Marsman, and G. Kresse, Zero-point renormalization of the band gap of semiconductors and insulators using the projector augmented wave method, Phys. Rev. B 106, 094316 (2022).
- [85] S. Logothetidis, J. Petalas, H. M. Polatoglou, and D. Fuchs, Origin and temperature dependence of the first

- direct gap of diamond, Phys. Rev. B 46, 4483 (1992).
- [86] J. E. Ortega and F. J. Himpsel, Inverse-photoemission study of ge(100), si(100), and gaas(100): Bulk bands and surface states, Phys. Rev. B **47**, 2130 (1993).
- [87] A. Evans, A. McGlynn, B. Towlson, M. Gunn, D. Jones, T. Jenkins, R. Winter, and N. Poolton, Determination of the optical band-gap energy of cubic and hexagonal boron nitride using luminescence excitation spectroscopy, Journal of Physics: Condensed Matter 20, 075233 (2008).
- [88] M. Piacentini, D. W. Lynch, and C. G. Olson, Thermore-flectance of lif between 12 and 30 ev, Phys. Rev. B 13,

- 5530 (1976).
- [89] R. Whited, C. J. Flaten, and W. Walker, Exciton thermoreflectance of mgo and cao, Solid State Communications 13, 1903 (1973).
- [90] L. Kavan, M. Grätzel, S. E. Gilbert, C. Klemenz, and H. J. Scheel, Electrochemical and photoelectrochemical investigation of single-crystal anatase, Journal of the American Chemical Society 118, 6716 (1996).